Materials for Proton Exchange Membrane Water Electrolyzer Bipolar Plates

Authors: Sigrid Lædre[a], Ole Edvard Kongstein[b], Anders Oedegaard[b], Håvard Karoliussen[a] and Frode Seland[a]

a Norwegian University of Science and Technology (NTNU), Norway

b SINTEF Materials and Chemistry, Norway

Corresponding author: Sigrid Lædre

Norwegian University of Science and Technology (NTNU)

7491 Trondheim

Norway

E-mail: Sigrid.ladre@gmail.com

Telephone: +47 97750663/ +47 73559637

Fax number: +47 73559631

Abstract

Titanium based Bipolar Plates (BPPs) are commonly used in Proton Exchange Membrane Water Electrolyzers (PEMWE) today as they can withstand the harsh operating conditions experienced inside an operating PEM water electrolyzer. In particular, the high anode potential and acidic nature of the PEM is crucial for BPP performance. In this work we expand the investigation of non-coated materials at relevant operating conditions to include molybdenum, 254 SMO, tungsten, AISI 316L, AISI 304L, Inconel 625, niobium and tantalum, in addition to Titanium gr. 2. Pre-designed potentiostatic and potentiodynamic tests at potentials up to 2.0 V_{SHE} were performed in addition to interfacial contact resistance (ICR) and weight loss measurements. Scanning Electron Microscopy (SEM) imaging was conducted to observe morphology changes during the electrochemical tests. Titanium, tantalum and niobium experienced little or no weight change during potentiostatic polarization, while for AISI 304L, AISI 316L and tungsten the measured weight loss was much lower than the weight loss calculated from currents produced. When the potentiostatic test was prolonged for titanium, the ICR was found to increase with time. Auger Electron Spectroscopy measurements confirmed that the increase in ICR for titanium, tantalum and niobium is related to an increased thickness of surface oxides.

1. Introduction

Hydrogen is considered one of the most promising energy carriers for the future [1-3], and is said to play an important role in storing of energy from renewable energy sources [4]. Today, hydrogen is predominantly produced by steam reforming of natural gas or gasification of coal and oil [1]. This method is a cost effective way of producing hydrogen, but simultaneously leads to significant carbon dioxide production impeding the transition to renewable and sustainable energy sources. Only about 4 % of the overall hydrogen production is done with water electrolysis [3]. On the other hand, production of hydrogen by electrolysis of water produces close to 100% pure hydrogen, is not dependent on fossil fuels and emits no carbon dioxide if produced with renewable energy. Alkaline water electrolysis has since its discovery in 1789 become the most common electrolyzer technology commercially available worldwide [1, 5, 6]. It is comprised of rather cheap components, has a very long life time at low maintenance costs and can be built into large units. It is, however, associated with a low partial load range, limited current density and low operating pressure [1].

Proton Exchange Membrane water electrolyzers (PEMWE) represent a zero-gap concept where a solid electrolyte, typically a humidified perfluorosulfonated polymer (Nafion®), is combined directly with two electrodes. The PEM electrolyzer is considered an interesting alternative to the alkaline water electrolyzer [1, 5, 7], as it can be operated under higher current densities and work under a wide range of power inputs [1]. The possibilities of dynamic operation of PEMWEs, including a load-following mode [1, 7], make them ideal in an energy capture and storage system for intermittent energy sources like wind, solar and wave, typically at remote locations. The membrane in the PEM electrolyzer provides high proton conductivity, low gas crossover and compact system design [1]. No liquid caustic electrolyte is circulated in the cell

stack, which makes the PEM electrolyzer both safer and more reliable compared to the alkaline electrolyzer [5].

An important component in a PEM electrolyzer stack is the Bipolar Plate (BPP) [4]. Its tasks are to separate single cells in a stack, conduct heat and current between single cells in a stack and distribute reacting agents within the electrolyzer [1, 4]. The BPP must have high corrosion resistance, possess high mechanical strength, high shock durability and be easy to manufacture allowing for mass production [4]. To the authors knowledge, there are currently no official targets for BPPs in PEMWEs, but the U.S. Department of Energy (DoE) [8] have set targets for BPPs in PEM fuel cells (PEMFCs). Their targets for 2020 include a maximum contact resistance of 0.01 Ω cm^2 and a maximum corrosion current density of 1 μA cm^{-2}. Even though these targets were developed for PEMFCs, low contact resistance and corrosion current is equally important for BPPs in PEMWEs, as they affect the cost, performance and lifetime. The BPP stand for a large fraction of the stack cost [1, 7], and a reduction of BPP manufacturing costs could thus drastically decrease the total cost of a PEMWE stack. The high single cell voltage and anode electrode potential, sometimes exceeding 2.0 V in an operating electrolyzer, restrains the materials selection significantly. Metal BPPs are in general easy to mass produce, and they exhibit exemplary electrical- and thermal properties. However, their tendencies of producing less conductive oxides on the metal surface can cause high ohmic resistance and poor performance. Titanium is typically used as BPP in PEM water electrolyzers today [1, 4], due to the high anodic potential and acidic environment during operation.

BPPs for PEMFCs have been thoroughly investigated [9-13], and in particular stainless steel BPPs [14-18]. In comparison, there are few published studies on BPPs for PEMWE. Titanium as BPP material in PEMWEs and regenerative fuel cells has been investigated to some extent [4, 19-24], with a main focus on coatings. Lin et al. [23] looked into the corrosion behavior of (Ti, Zr)N coated titanium for use as bipolar plate material in regenerative fuel cells. They found

the corrosion resistance of (Ti, Zr)N to outperform that of TiC, TiN and ZrN. Zang et al. [20] performed both corrosion-and Interfacial Contact Resistance (ICR) measurements on titanium with nanocomposite Ti-Ag-N. Zang et al. [19] investigated the corrosion properties, interfacial conductivity and surface energy of Ti-Ag coated titanium BPPs. They found the ICR to increase from 4.1 mΩ cm^2 to 22.2 mΩ cm^2 after polarization at 2.0 V_{SHE} for 4 hours.

Other materials have also been investigated for use as BPP material in electrolyzers [25-30]. Nikiforov et al. [25] tested the corrosion properties of several steel and nickel alloys in 85% phosphoric acid and at various temperatures for use in high temperature steam electrolyzers. Chisholm et al. [26] printed polypropylene flow plates for water electrolyzers by use of a 3D printer. They coated the printed plates with silver conductive paint. Gago et al. [27, 30] tested various titanium-based coatings, as well as surface modification with platinum on stainless steel BPPs for PEMWEs. Rasten et al. [29] suggested the use of highly alloyed stainless steel as BPP material for PEMEWEs. The recommended austenitic steel contained 20 weight % nickel, 20 weight % chromium, 3-5 weight % molybdenum, 0.5-2 weight % copper, 30-50 weight % iron and maximum 9 weight % other elements. Langemann et al. [28] measured the pH development over time on both anode and cathode side in a PEMWE equipped with corrosion resistant BPPs. They found the pH to decrease on both the cathodic and anodic side of the electrolyzer over a time span of 50 hours. The same authors performed polarization tests of AISI 304L coated with Au and TiN in a 0.50 M sulfuric acid solution at 2.0 V_{SHE}, and studied the pH development in the feeding water during these measurements.

Niobium, molybdenum, chromium and titanium have all been investigated as possible alloying components for stainless steel bipolar plates for fuel cells [31-33]. Kim et al. [33] investigated the alloying effects of Cr and Mo for several commercial steels, and found that the transpassive transition of stainless steels become progressively like the one for chromium as their Pitting

Resistance Equilibrium Number (PREN) increases. Feng et al. [31] found that by alloying AISI 316L with niobium, the dissolution rate of the material was significantly reduced.

A number of studies have been conducted with focus on the corrosion properties of metals such as AISI 316L, molybdenum, tungsten, niobium, tantalum, Inconel 625 and 254 SMO [34-43]. To the authors' knowledge, no studies have yet been published where both the corrosion properties and resistance development for a selection of relevant BPP materials have been collected at conditions similar to what the materials are exposed to inside a PEMWE. At high current operation, the potential experienced at an anode in a PEMWE can be even higher than 2.0 V_{SHE}. Corrosion studies rarely focus on testing materials at such high potentials, but it would be highly relevant in the field of PEM water electrolysis.

In this work the suitability of various relevant bipolar plate materials has been examined at potentials and pH relevant for PEMWE operation. Although the influence of hydrogen gas formation on bipolar plate stability and performance is of importance, we have limited our work to corrosion properties and interfacial contact resistance development of BPP materials exposed to conditions similar to those experienced on the anode side of an operating PEMWE. The materials were polarized as high as 2.0 V_{SHE}, making this study unique for several of these materials. This information is highly relevant in the selection of appropriate materials for BPPs in electrolyzers, including substrate materials for various coatings with the ultimate goal of reducing cost and increasing lifetime.

2. Procedure and Materials

The materials tested in this study are listed in Table 1. In addition to the procedures described below, a Hitachi S-3400N SEM was used for characterization. The accelerating voltage was kept at 15 kV for all the imaging. Prior to testing, the materials were etched in order to remove non-conducting oxides on the materials surface.

Table 1: Surface area and etching procedure of all the materials in this study.

Material	Surface area [cm^2] *	Etching agent	Etching time
Tungsten	3/5.4	37 % HCl	15 min
254 SMO	3.1/12.3	25 % HCl	15 min
Titanium gr. 2	12.3	37 % HCl	60 min
AISI 316L	3.1/12.3	12.5 % HCl	15 min
AISI 304L	3.1/3.1	12.5 % HCl	20 min
Tantalum	12.3	42 % KOH	24 h
Niobium	12.3	37 % HCl	15 min
Molybdenum	2.1/4.2	37 % HCl	15 min
Inconel 625	3.2/12.3	25 % HCl	15 min

* The given area is for one side of the test samples. For some of the materials, the samples used for potentiostatic and potentiodynamic measurements had different surface areas. The potentiostatic area is listed to the left and the potentiodynamic area is listed to the right.

Table 2: Compositions of the alloys used in this study.

Elements	Alloys and weight % of elements			
	AISI 316 L	**AISI 304L**	**254 SMO**	**Inconel 625 [46]**
Aluminum	-	-	-	0.4
Carbon	≤0.030	≤0.030	≤0.020	0.1
Chromium	16.0-18.0	18.0-20.0	19.5-20.5	20-23
Cobalt	-	-	-	1
Copper	-	-	0.5-1	-
Iron	Rest	Rest	Rest	5
Manganese	≤2.00	≤2.00	-	0.5
Molybdenum	2.0-3.0	-	6-6.5	8-10
Nickel	10.0-14.0	8.0-12.0	17.5-18.5	58
Niobium	-	-	-	3.15-4.15
Nitrogen	-	-	0.18-0.22	-
Phosphorus	≤0.045	≤0.045	-	-
Silicon	≤1	≤1	-	0.5
Sulfur	≤0.030	≤0.030	-	-
Titanium	-	-	-	0.4

The etching procedure for each material was adjusted in order to minimize the contact resistance after etching. The etching agent and time used to clean each material is listed in Table 1, along with the surface areas of each sample. The compositions of the alloys used in this work are listed in Table 2. In addition to the testing procedures described below, Scanning Electron Microscopy (SEM) and Auger Electron Spectroscopy (AES) was used to analyze the materials both before and after polarization.

2.1 Polarization

A Gamry ref 600 potentiostat with a three-electrode-setup was used to polarize the metal samples, as described by Lædre et al.[47] A Biologic VMP3 potentiostat was used for the high current experiments. The electrolyte used was a 0.1 M Na_2SO_4 solution that was adjusted to pH 5.5 by addition of 1 mM H_2SO_4. Platinum was used as counter electrode and Hg/Hg_2SO_4 electrode was used as the reference electrode. This reference electrode was deliberately chosen to ensure no chloride migration into the electrolyte. Chloride ions are known to cause aggressive pitting corrosion on e.g. AISI 316L stainless steel and possibly impair the platinum counter electrode. The reference electrode was kept in a saturated K_2SO_4 solution, and was connected to the electrolyte via a salt bridge with the same solution as the electrolyte. Nitrogen gas (5.0 N_2. Yara) was bubbled into the solution both before and during the polarization tests, to minimize oxygen content in the electrolyte.

The parameters used during the polarization tests are presented in Table 3. The potentiostatic test was designed to simulate the potential experienced by a bipolar plate inside an operating PEM water electrolyzer on the anode side. The potentiodynamic test was designed to show the corrosion properties of the metals when polarized between 0 and 2.0 V_{SHE}. These potentials were chosen to study the corrosion bipolar plates could experience inside a PEMWE. IR compensation was performed by employing the ohmic resistance obtained from an electrochemical impedance spectrum (EIS) obtained prior to each test.

Table 3: Polarization parameters chosen for the potentiostatic and potentiodynamic tests.

Test	Temperature [°C]	pH	Potential [V]	Duration /sweep rate
Potentiostatic	70	5.5	2.0 V_{SHE}	3600 s
Potentiodynamic	70	5.5	0-2.0 V_{SHE}	1.0 mV s^{-1}

All of the materials were weighed before and after polarization on an accurate laboratory scale, in order to obtain the weight loss.

2.2 Interfacial Contact Resistance

Before and after each polarization test, the interfacial contact resistance was measured ex-situ. The setup used for ICR measurement is shown in Figure 1. The ICR was measured between the specimen and a Gas Diffusion Layer (GDL, Freudenberg H23C6), where the GDL was used to measure the contact resistance towards a known, conductive material. The specimen with the GDL on top was put in between two gold-coated copper plates, and a pneumatic piston was used to move the lower plate towards the upper one. A current of 2.0 A was applied between the two gold coated copper plates by use of a XDL 56-4 DC power supply (Xantex). A pin connected to a very sensitive spring was mounted in the middle of the bottom plate, in order to obtain measurements at a certain area of the test specimen. The corresponding voltage was measured between the upper gold-coated copper plate and the spring loaded pin using a Fluke 76 True RMS multimeter, and this voltage was used to calculate the ICR between the specimen and the GDL.

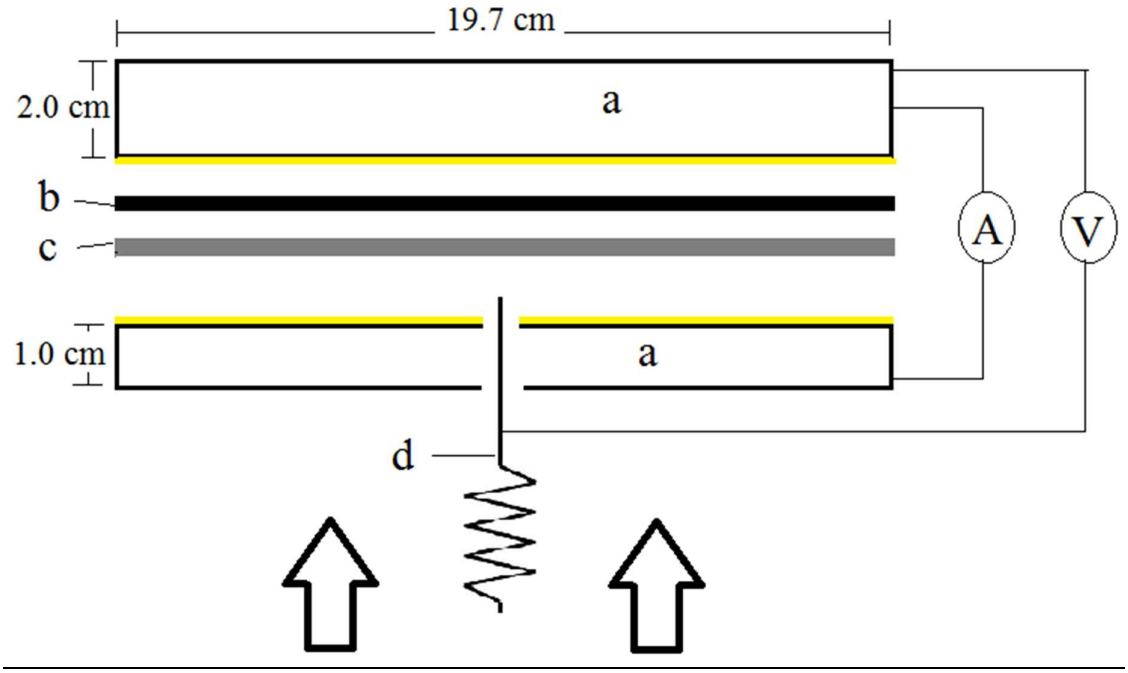

Figure 1

3. Results and Discussion

3.1 Potentiodynamic Polarization

The anode side of PEM water electrolysis bipolar plate is exposed to demanding conditions such as high positive potentials, acidic membrane and liquid water feed. . The conditions are significantly more demanding than for PEM fuel cells and polarization up to 2.0 V can be expected that may initiate other processes that one needs to be aware of. In addition to various corrosion reactions and oxide formation, oxygen evolution will also contribute to the overall current produced by the system.

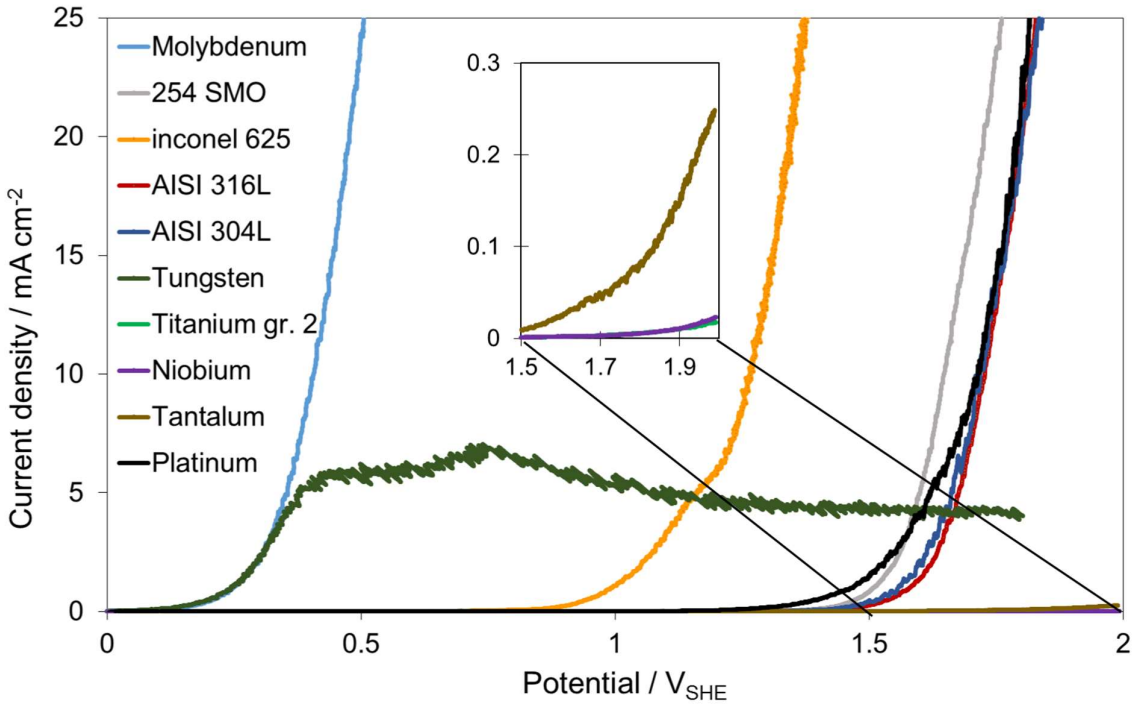

Figure 2

Figure 2 displays the current-potential relation obtained from the potentiodynamic tests performed for all the materials tested in this study. As several of the materials produced very high currents, all curves were cut at 25 mA cm^{-2}. Only the current onset and the initial current

increase behavior are emphasized upon in the comparison between the materials studied in this work. In addition to the various bipolar plate materials tested, a platinum wire was put through the potentiostatic test as well for comparison reasons. For simplicity we neglect any corrosion and conductivity changes due to Pt oxide formation during anodic polarization above 0 V_{SHE}, and thus assume that the current observed was attributed entirely to oxygen evolution. The current onset potential and initial current intensification during anodic polarization of the platinum electrode was then used to determine whether oxygen evolution or corrosion processes were the dominating process for the other sample materials.

Titanium, tantalum and niobium produced very low current densities throughout the entire sweep, with maximum current densities several order of magnitude lower than all the other materials in this study. The current density increased with increasing potential for all three materials. This increase could have been caused by corrosion, but it could also be a result of oxygen evolution on the sample surfaces.

For the molybdenum electrode, the current increased rapidly from approximately 0.25 V_{SHE}, and kept increasing throughout the entire test. This shows that accelerating current producing reactions took place on the material surface almost throughout the entire sweep. Oxygen evolution was to be expected only at higher potentials, in the same, or more positive potential region as oxygen evolution on the platinum electrode. Thus the early increase in current density at the molybdenum electrode, indicates corrosion processes occurring on the molybdenum surface during the early stages of the polarization. Not surprisingly, the same was also observed for the Inconel 625 sample, containing rather large amounts of both nickel and iron, known to corrode in acidic environment. However, it is worth noting that the observed current did not become excessive until about 1.0 V.

The three steel materials in this study, AISI 304L, AISI 316L and 254 SMO, did not show a clear current increase until approximately 1.5 V. A current increase at a lower potential was observed for the 254 SMO sample compared to the AISI 316L and AISI 304L steel samples. This was attributed to higher corrosion current at this sample, perhaps due to the higher fraction of molybdenum and nickel in this sample (Table 2). AISI 304L and AISI 316L were the two materials in this study with the most similar composition, and this is probably the reason why the curves for the two materials almost coincide in Figure 2. An interesting observation is that these same two steel materials produced currents very similar to platinum. This makes it difficult to determine which surface reactions that took place, as both oxygen evolution and corrosion processes were possible.

The potentiodynamic polarization of tungsten showed an increase in current density shortly after initiating the test, but then it stabilized at approximately 5.0 mA cm^{-2}. This is interesting, as none of the other materials experienced the same trend. One explanation could be that the rate-determining step for tungsten was a chemical reaction. Another explanation could be a limiting process strangling the current density to low values, for example slow dissolution of inactive oxide exposing the vulnerable metal underneath.

3.2 Potentiostatic Polarization

The results from the potentiostatic polarization tests are shown in Figure 3. Both niobium and tantalum are widely known for their ability to resist corrosion in most environments. This is attributed to the stable oxides formed on the metal surfaces of these metals [48, 49]. Compared to the other materials investigated in this study, niobium and tantalum produced very low currents. Potentiostatic polarization of tantalum resulted in current densities that stabilized around 10 µA cm^{-2}, while for niobium they stabilized around 20 µA cm^{-2}. Titanium, which is one of the most common substrate material used as BPPs in PEMWEs today [1], also showed

relatively low current densities (around 170 µA cm^{-2}) during the potentiostatic test. As with tantalum and niobium, titanium forms a stable oxide layer on the surface, which prevents corrosion. Tungsten produced currents higher than titanium, niobium and tantalum, but more than one order of magnitude lower than the rest of the materials. The currents from the polarization of tungsten stabilized at 3.7 mA cm^{-2}.

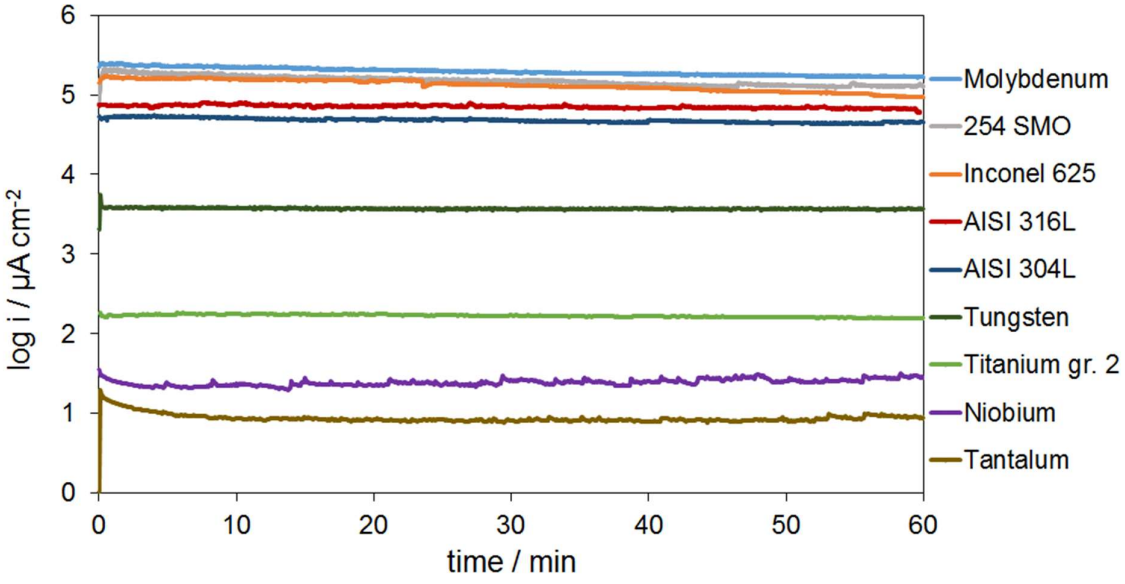

Figure 3

The material that produced the highest current densities during the potentiostatic test was molybdenum, with currents around 200 mA cm^{-2}. The potentiostatic polarizations of the steel samples AISI 316L, AISI 304L, 254 SMO and Inconel 625 all resulted in currents lower than molybdenum, but several orders of magnitude higher than tantalum, niobium, titanium and tungsten. The currents produced by these materials all decreased over time, where Inconel 625 showed a steeper decrease than the other materials. This change in current could arise from the formation and alteration of oxide composition on the metal surface. When comparing the results

in Figure 3 to the results in Figure 2, oxygen evolution cannot be excluded in the high currents observed for the AISI 304 and AISI 316L samples in Figure 3. For molybdenum, 254 SMO and Inconel 625, however, most of the contribution to the observed current densities is due to corrosion processes.

As for the potentiodynamic test, the potentiostatic polarization of tungsten resulted in current densities higher than titanium, but lower than the alloys. The current density kept stable at about 4 mA cm^{-2} throughout the entire polarization, which can be explained by a chemical dissolution process as the rate determining step [50]. Based on the current-potential behavior alone (Figures. 2 and 3), titanium, tungsten and tantalum appear to be the most promising BPP materials for PEM water electrolysis. However, the contact resistance for the various materials and its' development over time must also be considered before concluding. This is provided in section 3.4.

Figure 4 displays pictures after polarization (column 1) as well as SEM images obtained both before (column 3) and after polarization (column 2) of Inconel 625 and 254 SMO samples. The pictures and images from the potentiostatic polarizations of Inconel 625 (A) and 254 SMO (B) are shown, as well as the potentiodynamic polarization of 254 SMO (C). In all of the SEM images, heavy corrosion can be observed. The pictures and SEM images of the 254 SMO and Inconel 625 samples that had been put through the potentiostatic tests (Fig. 4 A1, A3, B1 and B3), revealed corroded surfaces, where corrosion had created deep cavities in the surface. The uneven structure of the sample surfaces indicates that a kind of non-uniform corrosion has happened. The corrosion may have been initiated as local pitting corrosion, inevitably progressing to the entire surface. Both of these materials have been found to experience pitting corrosion in certain environments [35, 51], even though they both should be pitting resistant in e.g. sea water [36, 52]. The picture and corresponding SEM image of the 254 SMO sample

obtained after the potentiodynamic polarization clearly displays pitting corrosion. This kind of corrosion can be very harmful to the material as it progresses rapidly once initiated.

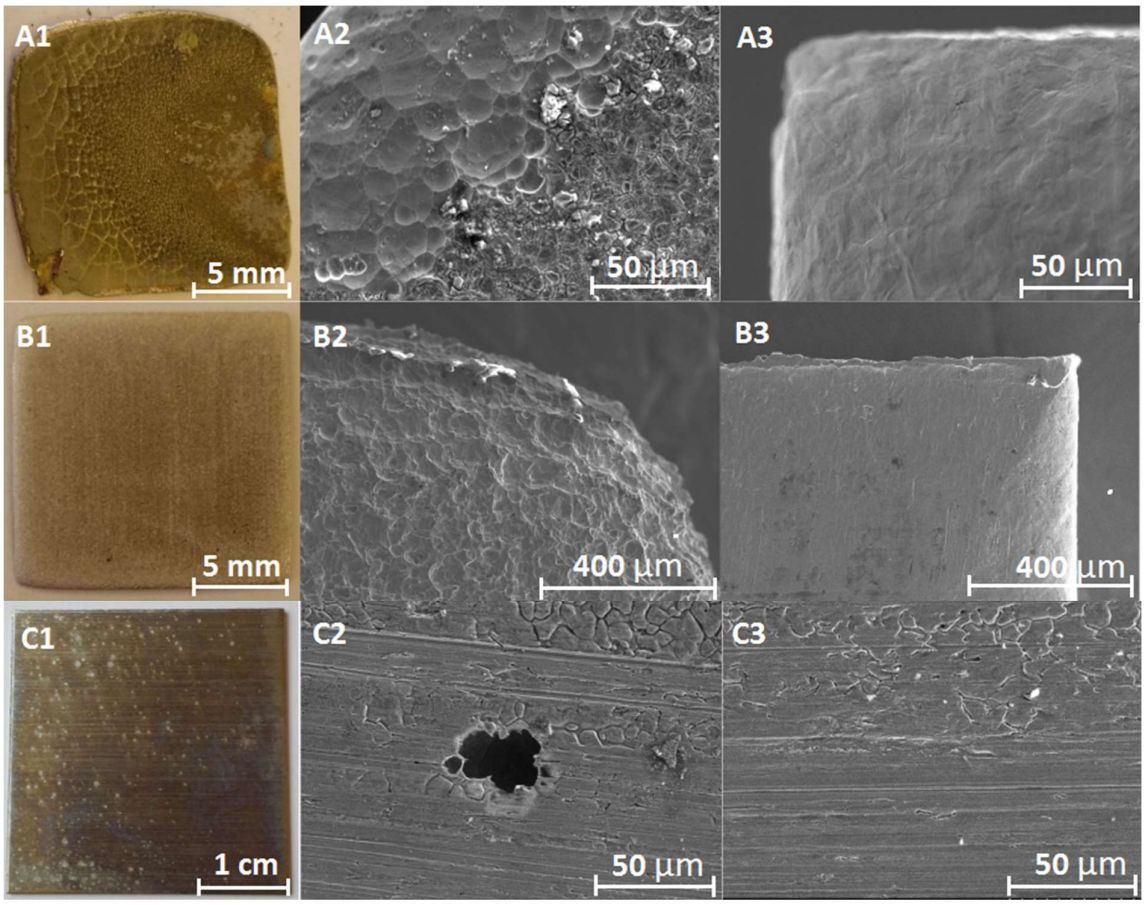

Figure 4

3.3 Corrosion and Weight Loss

Table 4 displays the results from weight measurements performed before and after each potentiostatic test, as well as weight calculations for each material from the current produced during polarization. By using Faradays law (equation 4) weight loss was calculated from the average currents produced by each material when polarized potentiostatically at 2.0 V_{SHE}. In this equation, m is the mass in grams, Q is the charge in Coulombs, M is the molar mass in grams per mole, F is Faradays constant in Coulombs per mole and n_{avg} is the average number of electrons transferred. The n_{avg} and molar masses for the alloys were calculated from the n and M values of all the components in the alloys.

$$m = \frac{Q \cdot M}{n_{avg} \cdot F}$$

Table 4: Weight loss measurements and calculations from the potentiostatic tests performed at 2 V_{SHE}, along with oxides from Pourbaix diagrams of the various materials at 25 °C and pH= 5.5 [53].

Material	Possible oxide(s)	n_{avg}	Measured weight loss [mg]	Estimated weight loss from total current [mg]	Percentage of current from corrosion [%]
Titanium gr. 2	TiO_2	4.0	-1.70[a]	1.83	-
Tantalum	Ta_2O_5	5.0	-2.70[a]	0.29	-
Niobium	Nb_2O_5	5.0	-27.00[a]	0.42	-
AISI 316L	$Fe_2O_3/Cr_2O_7^{2-}/NiO_2$	3.6	59.30	255.60	23.20
Tungsten	WO_3	6.0	5.00	25.52	19.59
AISI 304L	$Fe_2O_3/ Cr_2O_7^{2-}/NiO_2$	3.7	40.29	155.00	27.67
Molybdenum	MoO_3	6.0	530.30	506.00	104.80
254 SMO	$Fe_2O_3/ Cr_2O_7^{2-}/NiO_2$	3.9	609.20	518.70	117.50

Inconel 625	NiO_2/ $Cr_2O_7^{2-}$/Fe_2O_3	4.5	619.20	429.80	144.00

[a] The negative weight losses were probably cause by oxide development on the surface.

Also included in Table 4 are oxides retrieved from Pourbaix diagrams at 25 ºC, 2.0 V_{SHE} and pH=5.5 [53]. The temperature used during this study was higher than 25 ºC, but the content of Table 4 still proved valuable for the analysis performed here. For the alloy materials, the oxides from the major components are included. The oxide compositions on metal surfaces are complex, and the results in Table 4 are not based on an in depth study of the oxides of the materials in this work, as this was not the main objective here.

The percentage of current produced by corrosion was included in the table, with the objective of distinguishing between corrosion and other surface reactions, such as oxygen evolution. All components in an alloy were assumed to corrode simultaneously in the estimation of weight loss from the observed current. It was further assumed that the weight increase due to oxide formation was negligible in comparison to the total weight loss for most of the materials tested. However, for the materials with close to no weight loss the oxide formation at the surface of the material could be of significance in the weight measurements.

In fact, niobium, titanium and tantalum all experienced negative weight loss during the potentiostatic test (Table 4), which means they gained weight. Low corrosion combined with oxide formation, could explain the weight increase, as the weight gains were minor compared to the weight losses observed for the other materials. From Figures 2 and 3 it can be seen that the currents from both tantalum and niobium where low compared to most of the other materials, which indicates less corrosion.

Tungsten, AISI 304L and AISI 316L produced currents corresponding to weight losses approximately five times higher than the measured weight losses, when assuming that all the current came from corrosion. This indicates that most of the current came from oxygen

evolution, which is in agreement with the current-potential behavior reported in Figure 2 for the AISI 304L and AISI 316L steel samples. These curves almost overlap the one for platinum. The same trend was not observed for tungsten in the potentiodynamic test, but this does not exclude oxygen evolution, as the weight loss measurements were performed in conjunction with the potentiostatic tests.

The percentages of currents from corrosion were found to be more than 100% for 254 SMO, molybdenum and Inconel 625. All of these materials showed an increase in current at lower voltages than platinum in the potentiodynamic tests, and it is thus assumed that the contribution from corrosion was dwarfing the oxygen evolution. For molybdenum, the number is very close to 100, and the conclusion is that all of the current produced during the polarization, came as a result of corrosion. For 254 SMO and Inconel 625, the high percentage also shows that corrosion was responsible for all of the current. The fact that the percentage was above 100, can be explained by the difficulty in determining which elements in the alloy that contributed to the corrosion.

3.4 Interfacial Contact Resistance

Figure 5 shows how the measured contact resistance varied with pressure. ICR values at very low pressures proved to be difficult as some of the samples tested were much smaller than the equipment used for the ICR measurements. This is the reason why some of the curves in Figure 5 have different starting pressures. Figure 6 compares ICR values for all the materials at a pressure of 140 N cm^{-2} obtained before and after each onehour potentiostatic polarization. There are two bars for each material in Figure 6, where the one to the left shows the ICR value after sample pretreatment involving oxide removal, but before polarization. The bar to the right shows the ICR value obtained after the polarization measurements. The oxides on tantalum and niobium proved difficult to remove completely before polarization, which is reflected in the

relatively high ICR values for both materials before polarization. In order to understand these ICR results, it is important to compare them to the other measurements obtained in this study.

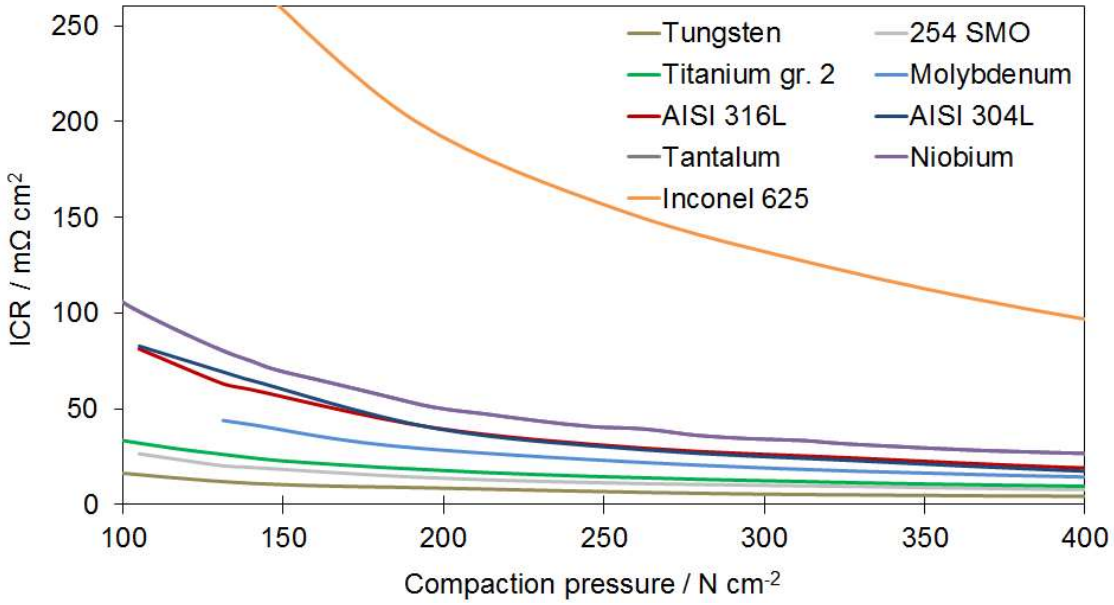

Figure 5

As can be seen from Figure 4.6, all materials, except tungsten, showed an increase in ICR after they had been polarized. In the case of tungsten, the ICR decreased from 13 mΩ cm^2 to 11 mΩ cm^2 after being polarized. We assume that this is due to a change of the tungsten surface, e.g. dissolution, resulting in a more conductive surface layer. Inconel 625 provided the highest ICR values after polarization (274 mΩ cm^2), while tungsten the lowest (11 mΩ cm^2). As the polarization and ICR measurements of Inconel 625 resulted in both high current densities and resistances, this material is a poor candidate for use as BPP in PEMWEs.

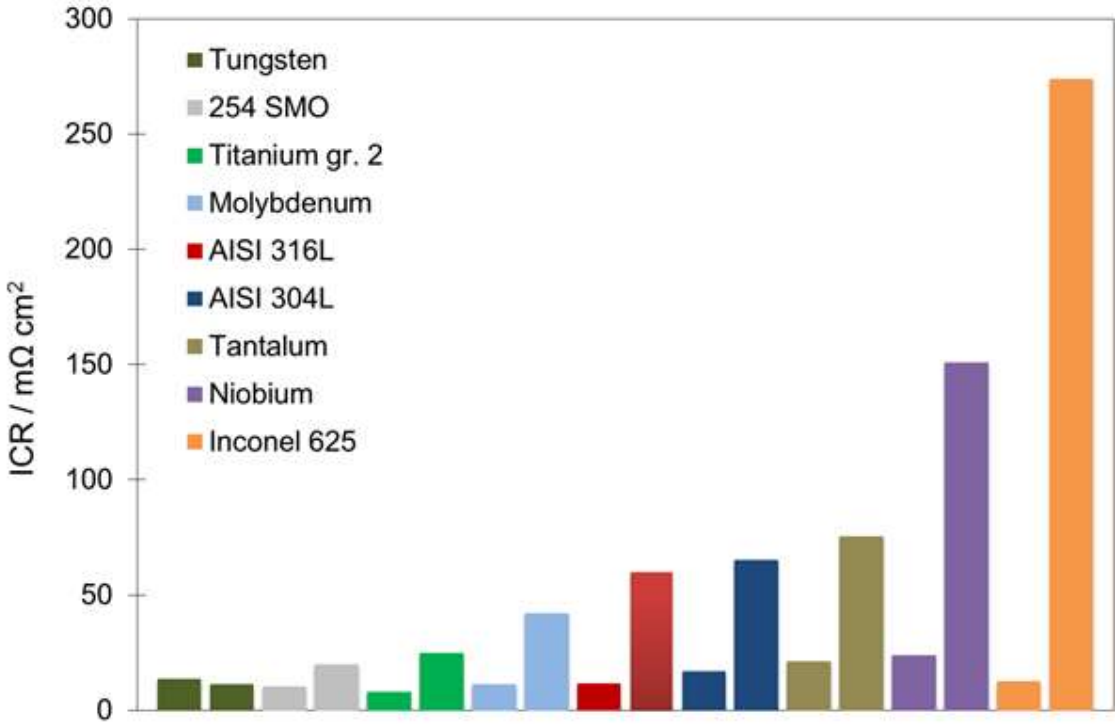

Figure 6

The ICR of titanium, tantalum and niobium went from 8 mΩ cm^2, 21 mΩ cm^2 and 24 mΩ cm^2 to 24 mΩ cm^2, 75 mΩ cm^2 and 151 mΩ cm^2 during polarization, respectively. This resulted in an increase of 3, 3.6 and 6.3 times the before-values. This corresponds well with the assumption that passive oxides are formed on their surfaces during anodic polarization. The negative weight loss measurements and low current densities in both potentiostatic and potentiodynamic polarizations for these three materials also strengthens this assumption.

AES analysis were performed on both polarized and unpolarized samples of titanium, tantalum and niobium. The polarized samples were the ones that had been polarized potentiostatically at 2 V_{SHE} for 1 hour, and the unpolarized samples were analyzed right after etching (Table 1). The results are presented in Figure 7.

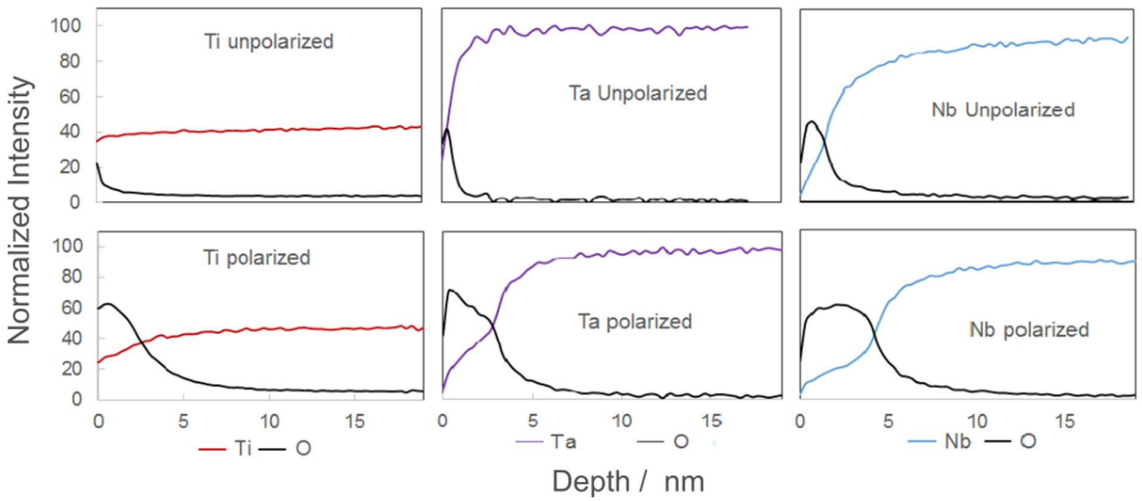

Figure 7

The AES results obtained from titanium, tantalum and niobium all show how the normalized intensity from the metals and oxygen vary with depth. The metal and oxygen form oxides on the surface of these materials, and the change in oxygen intensity reveals the thickness of the oxide. As can be seen from Figure 7, the oxygen peaks are wider after polarization compared to the unpolarized samples. This shows that the oxide is thicker after polarization, which helps explain the increase in ICR seen in Figure 6.

AISI 316L and AISI 304L produced currents in the same order of magnitude during both potentiostatic- and potentiodynamic polarization. The ICR values measured at 140 N cm^{-2} were 60 mΩ cm^2 for AISI 316L and 65 mΩ cm^2 AISI 304L. The main difference between these two materials is that the 316L steel contains molybdenum, while 304L does not. 254 SMO produced currents approximately one order of magnitude higher than both of the other steels, and the ICR value measured after polarization was 19 mΩ cm^2. High current density and low ICR indicate that this steel corroded more than 316L and 304L, and that the surface oxide formed was thinner or had a different composition than the other steels. 254 SMO contains higher amounts of both

molybdenum and nickel compared to both of the other steels, which could explain the difference in both current density and ICR.

The current densities from the potentiostatic polarization of tungsten were higher than for some of the other metals. This combined with a minimal ICR change, indicates that tungsten did not form a thick protective oxide during polarization. The Pourbaix diagram for tungsten at 25 °C suggests formation of either WO_3 or WO_4^{2-}, depending on concentration of ions [53]. All of the results combined support the idea that a reaction limiting process took place, which caused the low, but steady, current densities and the low ICR values for tungsten.

3.5 ICR Development over Time for Titanium

The duration of the potentiostatic test for titanium was prolonged to study how the ICR developed over time. Titanium samples were pretreated and put through a potentiostatic test at 2.0 V_{SHE} of various lengths. The resulting current densities and ICR values are displayed in Figure 8 and Figure 9, respectively. The absolute values of the current densities are all in the same order of magnitude, although slightly lower for the 122 h test indicating the expected variations at such low absolute values of the currents. The currents measured were all in the μA range, and at such low currents minor variations could lead to relatively large deviations. For all the tests the current density stabilized at the beginning of the tests, and kept stable throughout the test. For the 122 h test a very small increase in currents was observed towards the end of the test, but the low absolute values of the currents makes it difficult to determine whether it is a result of surface reactions or just instabilities in the measurements. The focus was thus put on the ICR measurements, which showed interesting development of the ICR over time. From the curve in Figure 9, it is evident that the ICR increased as the length of the test increased. This is crucial when considering titanium as a potential BPP material for PEMWEs. If the ICR

continues to increase, this would inevitably result in a continuous decrease in electrolyzer performance.

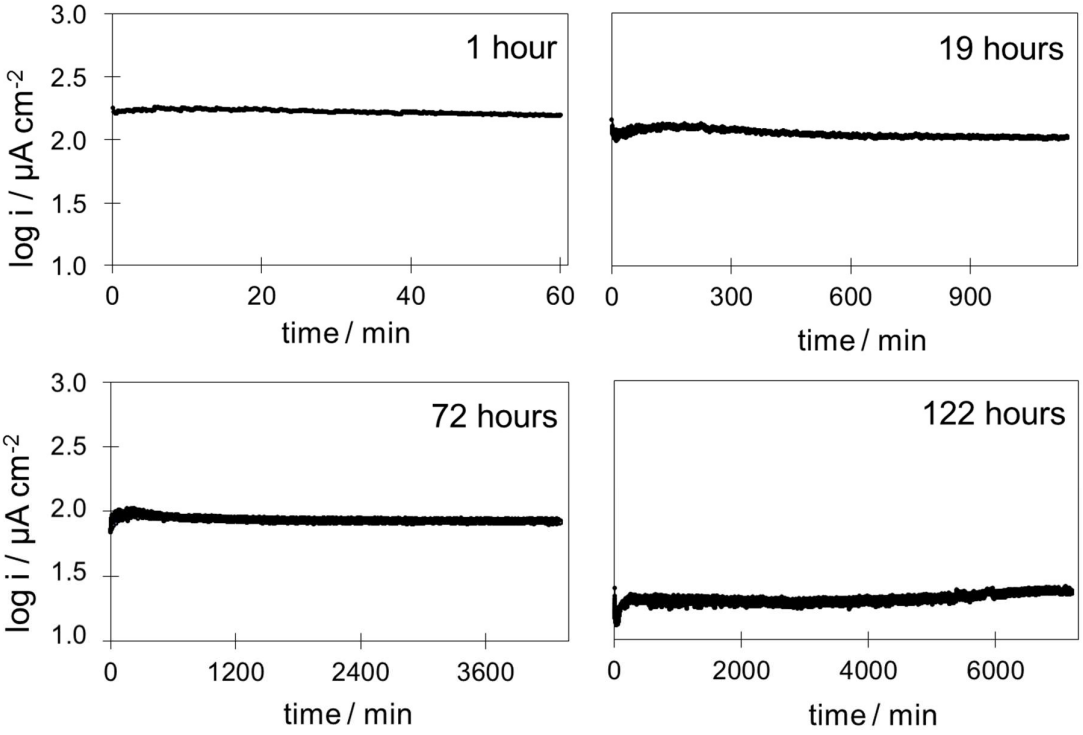

Figure 8

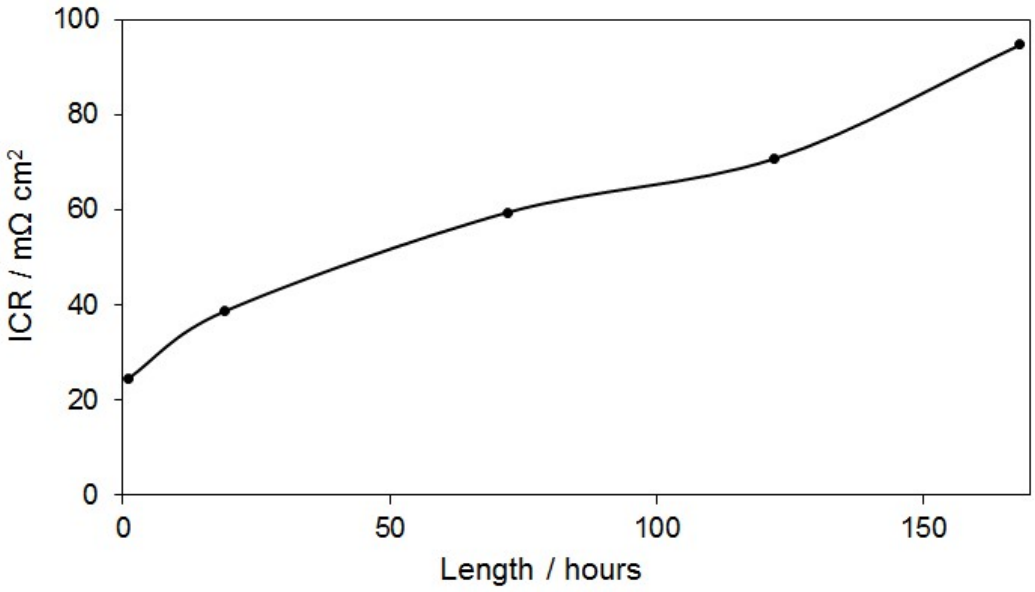

Figure 9

4. Conclusions

Corrosion properties and interfacial contact resistance development of a selection of non-coated bipolar plate materials have been tested at conditions relevant for PEM water electrolysis. In both the potentiostatic- and potentiodynamic polarization tests, tantalum, niobium and titanium produced low current densities compared to the other materials. Neither of these materials experienced any weight loss during polarization, which indicates that they did not corrode. On the other hand, both niobium and tantalum showed a significant increase in ICR, as compared to the negligible increase for titanium during the one-hour potentiostatic test. Nevertheless, prolonged polarizations at 2.0 V showed that the ICR increased also for titanium with time. AES analysis confirmed that the increase in ICR for titanium, tantalum and niobium could be attributed to the oxide layer growth on the material surface.

Weight measurements indicated that only approx. 20% of the overall current produced by the AISI 304L and 316L samples was related to corrosion. This suggests that these materials are

catalytically active towards oxygen evolution at 2.0 V. Even though some of the materials tested in this study, showed promising qualities, neither of them fulfilled the conductivity and corrosion requirements set by DoE for PEM fuel cells, which is likely to be a more strenuous benchmark if used for PEMWE. For both systems, it is crucial that the materials do not corrode or produce corrosion products that poison the electrolyte or electrocatalysts, and at the same time maintain a low interfacial contact resistance. Out of the tested materials titanium gr2 was the best performing material, with an excellent corrosion resistivity. However, a slow and continuous increase in the measured interfacial contact resistance during prolonged polarization points out the necessity of developing a conductive coating that limits the buildup of less conductive oxide, detrimental for PEM water electrolyzer performance. As there appears to be a lack of literature describing polarization up to 2.0 V_{SHE} for several of the materials tested in this study, the results presented here provide an important basis when choosing substrates for BPP coatings.

Acknowledgements

Financial support from the Norwegian University of Science and Technology (NTNU) and SINTEF materials and chemistry are greatly acknowledged. Additional interaction and support from the COATELY project is also acknowledged. Sigrid Lædre thanks NTNU for the award of a scholarship.

Literature

[1] Carmo M, Fritz DL, Mergel J, Stolten D. A comprehensive review on PEM water electrolysis. International Journal of Hydrogen Energy. 2013;38:4901-34.

[2] Barbir F. PEM electrolysis for production of hydrogen from renewable energy sources. Solar Energy. 2005;78:661-9.

[3] Dunn S. Hydrogen futures: toward a sustainable energy system. International Journal of Hydrogen Energy. 2002;27:235-64.

[4] Wang J-T, Wang W-W, Wang C, Mao Z-Q. Corrosion behavior of three bipolar plate materials in simulated SPE water electrolysis environment. International Journal of Hydrogen Energy. 2012;37:12069-73.

[5] Millet P, Andolfatto F, Durand R. Design and performance of a solid polymer electrolyte water electrolyzer. International Journal of Hydrogen Energy. 1996;21:87-93.

[6] Grigoriev SA, Millet P, Volobuev SA, Fateev VN. Optimization of porous current collectors for PEM water electrolysers. International Journal of Hydrogen Energy. 2009;34:4968-73.

[7] Ayers KE, Anderson EB, Capuano C, Carter B, Dalton L, Hanlon G, et al. Research Advances towards Low Cost, High Efficiency PEM Electrolysis. ECS Transactions. 2010;33:3-15.

[8] U.S. Department of Energy, *Fuel Cell Technologies Office Multi-Year Research, Development, and Demonstration Plan*. 2012. p. 29.

[9] Hermann A, Chaudhuri T, Spagnol P. Bipolar plates for PEM fuel cells: A review. International Journal of Hydrogen Energy. 2005;30:1297-302.

[10] Wang H, Turner JA. Reviewing Metallic PEMFC Bipolar Plates. Fuel Cells. 2010;10:510-9.

[11] Tawfik H, Hung Y, Mahajan D. Metal bipolar plates for PEM fuel cell - A review. Journal of Power Sources. 2007;163:755-67.

[12] Antunes RA, Oliveira MCL, Ett G, Ett V. Corrosion of metal bipolar plates for PEM fuel cells: A review. International Journal of Hydrogen Energy. 2010;35:3632-47.

[13] Hamilton PJ, Pollet BG. Polymer Electrolyte Membrane Fuel Cell (PEMFC) Flow Field Plate: Design, Materials and Characterisation. Fuel Cells. 2010;10:489-509.

[14] André J, Antoni L, Petit J-P. Corrosion resistance of stainless steel bipolar plates in a PEFC environment: A comprehensive study. International Journal of Hydrogen Energy. 2010;35:3684-97.

[15] André J, Antoni L, Petit J-P, De Vito E, Montani A. Electrical contact resistance between stainless steel bipolar plate and carbon felt in PEFC: A comprehensive study. International Journal of Hydrogen Energy. 2009;34:3125-33.

[16] Papadias DD, Ahluwalia RK, Thomson JK, Meyer Iii HM, Brady MP, Wang H, et al. Degradation of SS316L bipolar plates in simulated fuel cell environment: Corrosion rate, barrier film formation kinetics and contact resistance. Journal of Power Sources. 2015;273:1237-49.

[17] Wang HL, Sweikart MA, Turner JA. Stainless steel as bipolar plate material for polymer electrolyte membrane fuel cells. Journal of Power Sources. 2003;115:243-51.

[18] Yang Y, Guo L-j, Liu H. Corrosion characteristics of SS316L as bipolar plate material in PEMFC cathode environments with different acidities. International Journal of Hydrogen Energy. 2011;36:1654-63.

[19] Zhang H, Hou M, Lin G, Han Z, Fu Y, Sun S, et al. Performance of Ti–Ag-deposited titanium bipolar plates in simulated unitized regenerative fuel cell (URFC) environment. International Journal of Hydrogen Energy. 2011;36:5695-701.

[20] Zhang M, Hu L, Lin G, Shao Z. Honeycomb-like nanocomposite Ti-Ag-N films prepared by pulsed bias arc ion plating on titanium as bipolar plates for unitized regenerative fuel cells. Journal of Power Sources. 2012;198:196-202.

[21] Jung H-Y, Huang S-Y, Ganesan P, Popov BN. Performance of gold-coated titanium bipolar plates in unitized regenerative fuel cell operation. Journal of Power Sources. 2009;194:972-5.

[22] Jung H-Y, Huang S-Y, Popov BN. High-durability titanium bipolar plate modified by electrochemical deposition of platinum for unitized regenerative fuel cell (URFC). Journal of Power Sources.195:1950-6.

[23] Lin M-T, Wan C-H, Wu W. Comparison of corrosion behaviors between SS304 and Ti substrate coated with (Ti,Zr)N thin films as Metal bipolar plate for unitized regenerative fuel cell. Thin Solid Films. 2013;544:162-9.

[24] Toops TJ, Brady MP, Zhang F-Y, Meyer Iii HM, Ayers K, Roemer A, et al. Evaluation of nitrided titanium separator plates for proton exchange membrane electrolyzer cells. Journal of Power Sources. 2014;272:954-60.

[25] Nikiforov AV, Petrushina IM, Christensen E, Tomás-García AL, Bjerrum NJ. Corrosion behaviour of construction materials for high temperature steam electrolysers. International Journal of Hydrogen Energy. 2011;36:111-9.

[26] Chisholm G, Kitson PJ, Kirkaldy ND, Bloor LG, Cronin L. 3D printed flow plates for the electrolysis of water: an economic and adaptable approach to device manufacture. Energy Environ Sci. 2014;7:3026-32.

[27] Gago AS, Ansar SA, Saruhan B, Schulz U, Lettenmeier P, Cañas NA, et al. Protective coatings on stainless steel bipolar plates for proton exchange membrane (PEM) electrolysers. Journal of Power Sources. 2016;307:815-25.

[28] Langemann M, Fritz DL, Müller M, Stolten D. Validation and characterization of suitable materials for bipolar plates in PEM water electrolysis. International Journal of Hydrogen Energy.

[29] Rasten E, Hansen RS, Johnsen SE, Fell HJ. Use of Austenitic Stainless Steel as Construction Material in a Device or Structural Component Which is Exposed to an Oxygen and/or Hydrogen and/or Hydrofluoric Acid Environment. Patent application2010. p. Patent application number: 20100133096.

[30] Gago AS, Ansar AS, Gazdzicki P, Wagner N, Arnold J, Friedrich KA. Low Cost Bipolar Plates for Large Scale PEM Electrolyzers. ECS Transactions. 2014;64:1039-48.

[31] Feng K, Li Z, Cai X, Chu PK. Corrosion behavior and electrical conductivity of niobium implanted 316L stainless steel used as bipolar plates in polymer electrolyte membrane fuel cells. Surface and Coatings Technology. 2010;205:85-91.

[32] Lee S-H, Kim J-H, Kim M-C, Wee D-M. Effects of niobium and titanium addition and surface treatment on electrical conductivity of 316 stainless steel as bipolar plates for proton-exchange membrane fuel cells. Journal of Power Sources. 2009;187:312-7.

[33] Kim JS, Peelen WHA, Hemmes K, Makkus RC. Effect of alloying elements on the contact resistance and the passivation behaviour of stainless steels. Corrosion Science. 2002;44:635-55.

[34] Abd El Meguid EA, Abd El Latif AA. Electrochemical and SEM study on Type 254 SMO stainless steel in chloride solutions. Corrosion Science. 2004;46:2431-44.

[35] Abd El Meguid EA, Abd El Latif AA. Critical pitting temperature for Type 254 SMO stainless steel in chloride solutions. Corrosion Science. 2007;49:263-75.

[36] Cooper KP, Slebodnick P, Thomas ED. Seawater corrosion behavior of laser surface modified Inconel 625 alloy. Materials Science and Engineering: A. 1996;206:138-49.

[37] Fujii T, Sue K, Kawasaki S-i. Effect of pressure on corrosion of Inconel 625 in supercritical water up to 100 MPa with acids or oxygen. The Journal of Supercritical Fluids. 2014;95:285-91.

[38] Patrick E, Orazem ME, Sanchez JC, Nishida T. Corrosion of tungsten microelectrodes used in neural recording applications. Journal of Neuroscience Methods. 2011;198:158-71.

[39] Wang P, Wilson LL, Wesolowski DJ, Rosenqvist J, Anderko A. Solution chemistry of Mo(III) and Mo(IV): Thermodynamic foundation for modeling localized corrosion. Corrosion Science. 2010;52:1625-34.

[40] Zhu Y, Zhuang J, Zeng X. Mechanism of (NH4)S2O8 to enhance the anti-corrosion performance of MoCe inhibitor on X80 steel in acid solution. Applied Surface Science. 2014;313:31-40.

[41] Freitas MBJG, Eiras C, Bulhões LOS. Breakdown of the niobium oxide film under galvanostatic polarisation and in acid solutions. Corrosion Science. 2004;46:1051-60.

[42] Asselin E, Ahmed TM, Alfantazi A. Corrosion of niobium in sulphuric and hydrochloric acid solutions at 75 and 95 °C. Corrosion Science. 2007;49:694-710.

[43] Petrushina I, Nikiforov A, Bjerrum N, Petrushina I, Nikiforov A, Bjerrum N. Corrosion behavior of highly austenitic stainless steels and Ni-based alloys at elevated temperatures in concentrated phosphoric acid solutions. International Conference on Hydrogen Material Science and Chemistry of Carbon Nanomaterials, August 25-31, 2009, Yalta, Ukraine. 2009:162-3.

[44] Bernstein IM, Peckner D. Handbook of stainless steels. New York: McGraw-Hill; 1977.

[45] Covino BS, Cramer SD. Corrosion : fundamentals, testing and protection. [Rev. ed.]. ed. Materials Park, OH: ASM International; 2003.

[46] Committee ASMIH. ASM Handbook, Volume 02 - Properties and Selection: Nonferrous Alloys and Special-Purpose Materials. ASM International; 1990. p. 1118-28.

[47] Lædre S, Kongstein OE, Oedegaard A, Seland F, Karoliussen H. The effect of pH and halides on the corrosion process of stainless steel bipolar plates for proton exchange membrane fuel cells. International Journal of Hydrogen Energy. 2012;37:18537-46.

[48] Revie RW, Uhlig HH. Tantalum. Corrosion and Corrosion Control: John Wiley & Sons, Inc.; 2008. p. 441-3.

[49] Mishra B. Review of Extraction, Processing, Properties, and Applications of Reactive Metals : 1999 TMS Annual Meeting, San Diego, CA, February 28-March 15, 1999. Somerset, NJ, USA: John Wiley & Sons; 2013.

[50] Drazic DM, Popic JP. Anomalous dissolution of metals and chemical corrosion. Journal of the Serbian Chemical Society. 2005.

[51] Scully JR, Kehler BA, Ilevbare G. Crevice Corrosion Stabilization and Repassivation Behavior of Alloys 625 and 22. NACE International.

[52] Olsson J, Wallen B. Experience with a high molybdenum stainless steel in saline environments. Desalination. 1983;44:241-54.

[53] Pourbaix M. Atlas of electrochemical equilibria in aqueous solutions. Oxford; New York: Pergamon Press; 1966.